Applied Catalysis B: Environmental 94 (2010) 288–294

Contents lists available at ScienceDirect

Applied Catalysis B: Environmental

journal homepage: www.elsevier.com/locate/apcatb

Kinetics and mechanism of advanced oxidation processes (AOPs) in degradation of ciprofloxacin in water

Taicheng An [a,*], Hai Yang [a,b], Guiying Li [a], Weihua Song [c], William J. Cooper [c], Xiangping Nie [d]

[a] State Key Laboratory of Organic Geochemistry and Guangdong Key Laboratory of Environmental Resources Utilization and Protection, Guangzhou Institute of Geochemistry, Chinese Academy of Sciences, Wushan Street, Tianhe District, Guangzhou 510640, China
[b] Graduate School of Chinese Academy of Sciences, Beijing 100049, China
[c] Urban Water Research Center, Department of Civil and Environmental Engineering, University of California, Irvine, Irvine, CA 92697-2175, United States
[d] Institute of Hydrobiology, Jinan University, Guangzhou 510632, China

ARTICLE INFO

Article history:
Received 23 September 2009
Received in revised form 24 November 2009
Accepted 1 December 2009
Available online 4 December 2009

Keywords:
Ciprofloxacin
Advanced oxidation processes
Photocatalytic
Kinetics
Mechanism

ABSTRACT

Fluoroquinolones and their metabolites are found in surface and ground waters, indicating their ineffective removal by conventional water treatment technologies. Advanced oxidation processes (AOPs) are alternatives to traditional water treatments. They utilize free radical reactions to directly degrade fluoroquinolones. This work reports absolute rate constants for the reaction of ciprofloxacin with several free radicals, $^{\bullet}OH$, $^{\bullet}N_3$ and $SO_4^{\bullet-}$ as well as hydrated electrons. Pulsed radiolysis experiments showed that $^{\bullet}OH$, $^{\bullet}N_3$ and e_{aq}^- reacted quickly with ciprofloxacin, with bimolecular reaction rate constants of $(2.15 \pm 0.10) \times 10^{10}$, $(2.90 \pm 0.12) \times 10^{10}$ and $(2.65 \pm 0.15) \times 10^{10}\ M^{-1}\ s^{-1}$, respectively, while the $SO_4^{\bullet-}$ radical appeared not to react with ciprofloxacin. Transient spectra were observed for the intermediate radicals produced by hydroxyl and azide radical reactions. Moreover, ciprofloxacin can be degraded rapidly using a typical advanced oxidation process, TiO_2 photocatalysis, with half-lives of 1.9–10.9 min depending upon pH values. Seven degradation products were elucidated by LC/MS/MS analysis, and the degradation mechanism of ciprofloxacin was also tentatively proposed by combining the experimental evidence with theoretical calculations of frontier electron densities. The calculations suggest that the addition of a hydroxyl radical to ciprofloxacin and photo-hole direct attack is two predominant reaction pathways.

1. Introduction

The sources, occurrence, fate, effects and risks of pharmaceuticals in the environment are issues of increasing importance [1,2]. Pharmaceutical compounds cover a wide range of compounds with substantial variability in structure, function, behavior and activity, and are used in both humans and animals to cure disease and fight infection [3]. The fluoroquinolone group is one of the most important pharmaceuticals used worldwide for humans and veterinary purposes [4]. Several recent studies have reported the environmental presence of fluoroquinolones in many countries, such as Switzerland, the United States, Australia and China [4–7]. The presence of broad spectrum antibiotics like these in aquatic environments, albeit at low concentrations, may pose serious threats to the ecosystem and human health by inducing proliferation of bacterial drug resistance [6,8].

Most fluoroquinolones are not fully metabolized in the body and so may be excreted [6] and entered the environment through wastewater effluents [9]. Thus, alternative physiochemical technologies are needed to minimize environmental discharges [6,10,11]. Advanced oxidation processes (AOPs), with the highly reactive hydroxyl radical ($^{\bullet}OH$) as the main oxidative species, are an alternative for degrading these soluble bio-refractory human antibiotics (fluoroquinolone group) [12,13]. However, not so many studies focusing on the photodegradation possibilities and the degradation kinetics of fluoroquinolone have been reported [14,15].

Studies on the photodegradation of fluoroquinolones [16–18], ozone oxidation [19] and transformation of fluoroquinolones with manganese oxide [4] have been reported. However, to date, no systemic studies concerning the radical-based (hydroxyl radical and hydrated electron (e^-_{aq}) as well as azide radical ($^{\bullet}N_3$) and sulfate radical ($SO_4^{\bullet-}$)) reaction kinetics and mechanism of ciprofloxacin (CIP) have been reported. Insight into the fundamentals of the free radical chemistry reaction of CIP will enhance the development of strategies to control and target selective chemical transformation for environmental applications.

This study reports the absolute kinetics and efficiencies of hydroxyl radical and hydrated electron reactions as well as azide

* Corresponding author. Tel.: +86 20 85291501; fax: +86 20 85290706.
E-mail address: antc99@gig.ac.cn (T. An).

0926-3373/$ – see front matter © 2009 Elsevier B.V. All rights reserved.
doi:10.1016/j.apcatb.2009.12.002

radical and sulfate radical reactions with CIP. To properly assess the risk of CIP in aqueous solution and better understand its environmental fate and the transformation of fluoroquinolone pharmaceuticals in real water systems, heterogeneous photocatalytic oxidation technology was selected as a representative AOP. The frontier electron densities of CIP were also calculated, to predict the first reaction position with a hydroxyl radical and photo-hole attack in the photocatalytic degradation mechanism of CIP.

2. Experimental

2.1. Materials

CIP was purchased from Sigma–Aldrich (>98% purity) and used without further purification. Solutions for irradiation were prepared using filtered water from a Millipore Milli-Q system, while the solution for the photocatalytic degradation experiments was prepared with double-distilled water. The irradiation kinetics solutions were sparged with high-purity N_2O (for hydroxyl radical experiments) or N_2 (for hydrated electron and $SO_4^{\bullet-}$ experiments) to remove dissolved oxygen.

2.2. Pulse radiation

Electron pulse radiolysis experiments were performed at the Notre Dame Radiation Laboratory using the 8-MeV Titan Beta model TBS-8/16–1S linear accelerator with pulse lengths of 2.5–10 ns. A typical experiment consisted of a series of 6–10 replicate shots which were averaged for a single measurement. Dosimetry [20] was performed using N_2O-saturated 10 mM KSCN solutions at $\lambda = 472$ nm, $((G\epsilon) = 5.2 \times 10^{-4}\ m^2\ J^{-1})$ with average doses of 3–5 Gy per 2–3 ns pulse. Throughout this paper, the units of G are $\mu mol\ J^{-1}$, and ϵ is in units of $M^{-1}\ cm^{-1}$. All experimental data were determined by averaging 8–12 replicate pulses using the continuous flow mode of the instrument. The radiolysis of water is described in Eq. (1) [21–23], where the numbers in parentheses are the G-values in $\mu mol\ J^{-1}$.

$$H_2O \rightarrow e_{aq}^{-}\,[0.27] + {}^{\bullet}H\,[0.06] + {}^{\bullet}OH\,[0.28] + H_2\,[0.05] + H_2O_2\,[0.07] + H^{+}\,[0.27] \quad (1)$$

2.3. Photocatalytic experiments

The adsorption and photocatalytic degradation of CIP was carried out in a Pyrex tube (150 mL) with a double-walled cooling water jacket to keep the temperature of solutions constant with 25 ± 1 °C throughout the experiments. The light source, which was a high-pressure mercury lamp (GGZ-125, Shanghai Yaming Lighting, $E_{max} = 365$ nm) with a power consumption of 125 W, was housed in one side of the photocatalytic reactor to provide the irradiation. The light intensity at the surface of Pyrex tube was achieved at the average of 0.38 mW cm^{-2}. Prior to illumination, a suspension of 150 mL CIP (100 μM) with 1.5 g/L photocatalyst (Degussa P25) was stirred in the dark for 30 min to achieve the adsorption–desorption equilibrium. The UV light was then turned on for the photocatalytic degradation experiments. 3 mL of CIP solution was sampled at fixed intervals, filtered through a 0.2 μm Millipore filter and used for HPLC and HPLC/MS/MS analysis.

2.4. HPLC and LC/MS/MS analysis

CIP and its reaction products were analyzed by Agilent 1200 series HPLC under the following conditions: a Phenomenex Gemini C18 column, 250 mm × 4.6 mm i.d., was used for chromatographic separations at 30 °C. The mobile phase, acetonitrile/phosphoric acid (pH = 2.3, 20 mM) mixed solution (20:80, v/v) containing 2.5 mM 1-heptanesulphonic acid sodium salt, was vacuum filtered with a Water Associates (Milford, MA, USA) filtering kit, $\varphi = 0.45$ μm. The mobile phase was set at 1.0 mL min^{-1}, and the detection wavelength was set at 278 nm.

HPLC/MS/MS: A Shimadzu high performance liquid chromatography (HPLC) system with a Phenomenex Gemini C18 column, 250 mm × 4.6 mm i.d, an SIL-HT autosampler, LC-10 ATvp pumps and an API 3000 mass analyzer was used. HPLC separations were performed at 0.5 mL min^{-1} using injection volumes of 20 μL and linear gradient elution as follows: the initial 93% A (0.03% (v:v) formic acid solvent) and 7% B (acetonitrile) mobile phase was changed to 50% A and 50% B over 25 min, and then returned to the initial conditions over a further 25 min. An electro-spray interface was used for the MS and MS/MS measurements in positive ionization mode and full scan acquisition [24]. The collision energy varied according to the requirements of the different measurements, and the other parameters were set as follows: the ESI was set at 5.5 kV, the source block and desolvation temperatures were 130 °C and 400 °C, respectively, the desolvation and nebulizer gas (N_2) flow rate were set at 6 L min^{-1} and argon gas was used as a collision gas at 2500 mbar.

2.5. Calculation of frontier electron density of CIP

Molecular orbital calculations were carried out at the single determinant (HF/3-21) level with the optimal conformation having a minimum energy obtained at the B3LYP/6-31G* level in a Gaussian 03 system on a personal computer. Structures were optimized at the level of unrestricted Gaussian Viewer software using Hartree–Fock for all calculations. The frontier electron densities (FEDs) of the highest occupied molecular orbital (HOMO) and the lowest unoccupied molecular orbital (LUMO) were determined [25,26]. Values of both $2FED^2_{HOMO}$ and $(FED^2_{HOMO} + 2FED^2_{LUMO})$ were calculated to predict the reaction sites for electron extraction and hydroxyl addition, respectively.

3. Results and discussion

3.1. Free radical mediated degradation of CIP

3.1.1. Reaction with hydroxyl radical

To study only the reactions of the •OH, solutions were presaturated with nitrous oxide (N_2O), which quantitatively converts hydrated electrons and hydrogen atoms to hydroxyl radicals, as described elsewhere [27]. The absolute bimolecular reaction rate constants were determined in 50 μM solutions of CIP without buffering. With the proceeding of the reaction between hydroxyl radical with CIP, the increasing time-resolved transient absorption spectra were observed and the profiles at different reaction time intervals were recorded in Fig. 1. Two isosbestic points were observed and a highest peak in the absorptions range of the transient profile was formed at 290 nm. The lifetime of this transient species was on the scale of 5 μs, and then this transient will decay very quickly. The typical growth kinetic curve of OH-adduct is plotted in Fig. 2. The bimolecular rate constant for the reaction of CIP with •OH radical, can be determined from the linear dependence of the first-order growth rate constant on the CIP concentration (inset of Fig. 2). The rate constant with •OH radicals was obtained as $(2.15 \pm 0.10) \times 0^{10}\ M^{-1}\ s^{-1}$. Thus we can also conclude that the •OH radicals are highly reactive toward CIP and attacked with a diffusion controlled rate ($k > 10^9\ M^{-1}\ s^{-1}$) although there are still no any information on the rate constant for CIP in the early reported references.

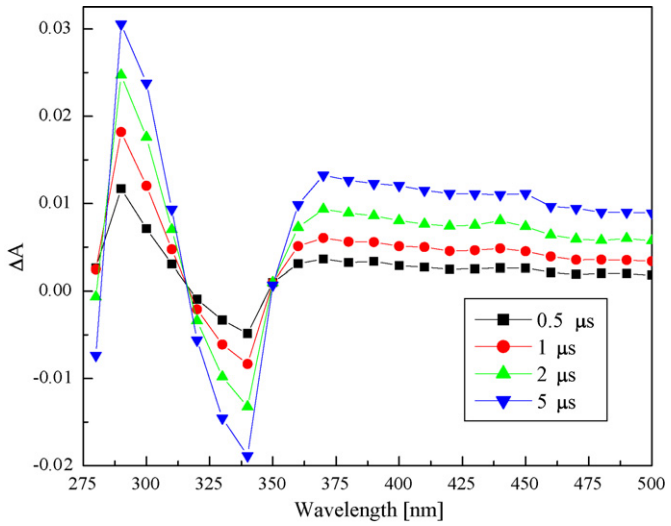

Fig. 1. Transient spectrum obtained upon the hydroxyl radical (•OH) oxidation of CIP in N_2O-saturated pH 7.0 solutions at room temperature for 0.5 (■), 1.0 (●), 2.0 (▲) and 5.0 (▼) μs time intervals.

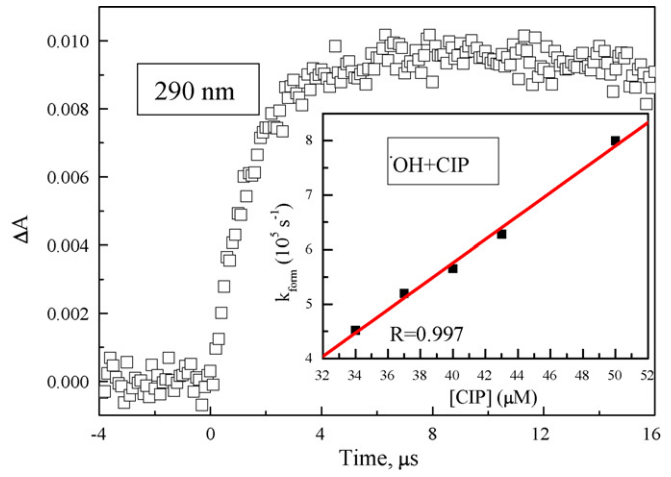

Fig. 2. The build-up of intermediate at 290 nm in a pulse-irradiation solution of CIP with concentration of 50 μM in N_2O-saturated pH 7.0 solution. Inset: plot of the first-order transient formation rate constant at 290 nm vs different CIP concentrations in the reaction with •OH radical.

3.1.2. Reaction with azide (•N_3) and sulfate ($SO_4^{\bullet-}$) radicals

To further understand the possible electron-transfer mechanism of radical reactions, the reactions of CIP with azide (•N_3) and sulfate ($SO_4^{\bullet-}$) radicals were also studied. The reactions of CIP with these oxidizing radicals would allow comparison of these oxidation processes with that of •OH radicals.

The azide radical •N_3 can be easily formed by pulse radiolysis of sodium azide solution (0.01 M) saturated with N_2O gas as described in Eq. (2). The azide radical is a mild oxidant (E^0 = 1.33 V vs NHE) [28]. It is more selective than a hydroxyl radical and easily participates in one-electron oxidation via primary formation of radical cations [21,29]:

$$N_3^- + {}^\bullet OH \rightarrow {}^\bullet N_3 + OH^- \quad (k = 1.2 \times 10^{10}\ m^{-1}\ s^{-1}) \qquad (2)$$

The azide radical has a sharp adsorption at ~274 nm and very little adsorption above 300 nm in the absence of a suitable reductant in the solution [27]. In our experiments, a solution containing 10 mM NaN_3 and 50 μM CIP was mixed at a pH value 7.0 for the reaction of azide radicals with CIP. A peak around at

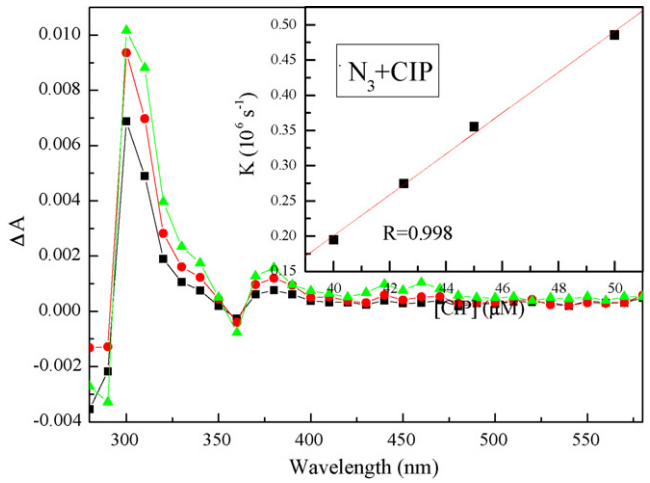

Fig. 3. Difference adsorption spectra of the transient generated from the reaction of 50 μM CIP, saturated with N_2O, at pH value 7.0 and 10 mM NaN_3 at 0.5 (■), 1.0 (●), and 2.5 (▲) μs time intervals. Inset: plot of the first-order transient formation rate constant at 300 nm vs different CIP concentrations in the reaction with azide •N_3 radical.

300 nm was observed at the transient adsorption spectra, and the peak also increases rapid with the extensions of the irradiation time within 2.5 μs (showed in Fig. 3). The peak at 300 nm was used to evaluate the reaction rate constant with the azide radical and the regression of pseudo-first-order rate constants is shown in the inset in Fig. 3. The slope of the inset plot is the second-order rate constant for the reaction between •N_3 radical and CIP obtained as $(2.90 \pm 0.12) \times 10^{10}\ M^{-1}\ s^{-1}$. This measured rate constant with •N_3 radical is almost the same order of magnitude as that of •OH radical, which indicated that CIP is prone to oxidize by less active oxidizing radicals than the hydroxyl radical, and can easily occur the one-electron transfer reaction with the •N_3 radical.

The sulfate radical, $SO_4^{\bullet-}$, is a very strong oxidant (E^0 = 2.43 V vs NHE) [30] and also can react via electron transfer. $SO_4^{\bullet-}$ was formed by the reaction of a persulfate dianion (10 mM) with a solvated electron in N_2-saturated solutions as shown in Eq. (3), with a yield of G ($SO4^{\bullet-}$) = 2.7:

$$S_2O_8^{2-} + e^-_{aq} \rightarrow SO_4^{2-} + SO4^{\bullet-} \ (2.7) \qquad (3)$$

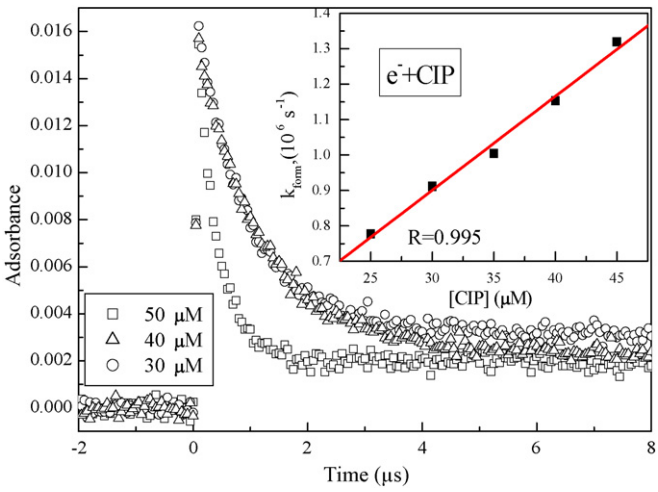

Fig. 4. Typical decay kinetics of hydrated electron adsorption at 700 nm for 30 (○), 40 (△) and 50 (□) μM CIP at pH value 7.0. Inset: plot of the first-order transient formation rate constant at 700 nm vs different CIP concentrations in the reaction with hydrated electron.

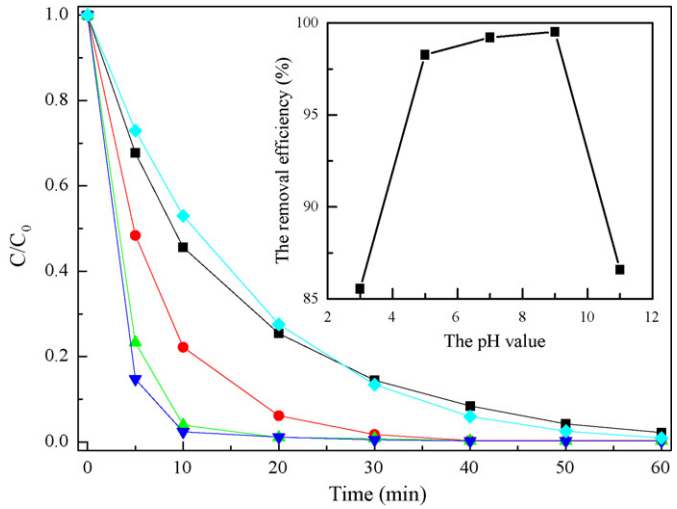

Fig. 5. Photocatalytic degradation efficiencies of 100 μM CIP with 1.5 g L^{-1} photocatalyst concentration, at 3.0 (■), 5.0 (●), 7.0 (▲), 9.0 (▼) and 11.0 (◆) pH values. Inset: effect of pH values on the efficiencies of photocatalytic degradation of 100 μM CIP at 30 min interval.

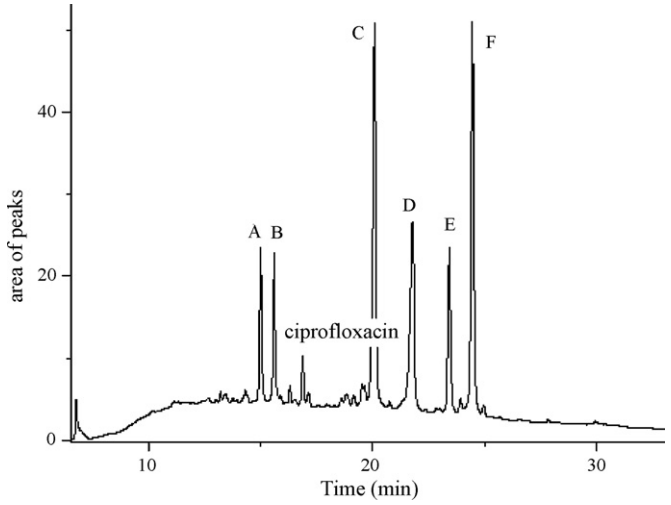

Fig. 6. HPLC chromatogram of the photocatalytic degradation of ciprofloxacin for 40 min. Peaks A to F: degradation compounds.

Hydroxyl radicals were removed by the addition of *tert*-butyl alcohol (0.1 M) to the solution. The transient adsorption spectra of 50 μM CIP did not show any significant adsorption in the 250–500 nm wavelength regions. A weak adsorption change ($\Delta A < 0.003$ at 300 nm) was obtained in the irradiation experiments (not shown), which was indicative of the low reactivity of CIP toward the $SO_4^{\bullet-}$ radical. This phenomenon why CIP have so low reactivity with the $SO4^{\bullet-}$ radical must need further experiments to elucidate in the near future.

3.1.3. Reaction with hydrated electron

To isolate hydrated electron reactions, solutions were presaturated with nitrogen in the presence of 0.1 M *tert*-BuOH to scavenge the hydroxyl radicals and hydrogen atoms, converting them into relatively inert *tert*-butyl alcohol radicals [31]. No significant transient was observed from 250 nm to 800 nm following the reaction of the hydrated electron with CIP. Thus the rate constant for the hydrated electron reaction with CIP was measured by directly monitoring the decrease of the absorption of hydrated electrons at 700 nm in nitrogen-saturated solutions.

The typical decay kinetic profiles are illustrated in Fig. 4. The decay curves were fitted to pseudo-first-order exponential kinetics and the second-order linear plot was shown in the inset of Fig. 4. The slope of such a plot is the second-order rate constant for hydrated electron reduction of CIP obtained as $(2.65 \pm 0.15) \times 10^{10}$ M^{-1} s^{-1}. Although no reduction rate constant for CIP reaction with hydrated electron was reported in the previously published references, we can easily see the rate constant is the same order of magnitude as that of other environmental pharmaceuticals, such as beta-blockers [22].

3.2. Photocatalytic degradation kinetics of CIP

The photocatalytic degradation of CIP was investigated at the optimal TiO_2 concentration of 1.5 g L^{-1}. This concentration was determined by our primary experiments for selecting a photocatalyst concentration. The degradation of CIP was significantly affected by pH values as reflected by the photocatalytic efficiencies (inset in Fig. 5). The photocatalytic degradation was linearly plotted as pseudo-first-order degradation kinetics and was consistent with the Langmuir–Hinshelwood (L–H) model. The rate constants and half-times at different pH values are listed in Table 1. The rate constants increased from 0.06 min^{-1} at pH 3.0 to 0.38 min^{-1} at pH 9.0, and then decreased to 0.07 min^{-1} at pH 11.0. On the other hand, the half-time decreases from 10.9 min at pH 3.0 to 1.9 min at pH 9.0, and then increases to 9.4 min at pH 11.0 again. The high rate constants and short half-lives at various pH values suggest that CIP can undergo fast photocatalytic degradation.

Table 1
Photocatalytic degradation rate constants and half-lives of CIP at various pH values.

pH value	Confidence coefficient	Rate constant (min^{-1})	Half-time (min)
3.0	0.999	0.06 ± 0.01	10.9
5.0	0.999	0.14 ± 0.01	4.9
7.0	0.975	0.25 ± 0.02	2.8
9.0	0.999	0.38 ± 0.01	1.9
11.0	0.997	0.07 ± 0.01	9.4

These results are likely the result of two effects. The isoelectric point of TiO_2 is approximately 6.3. Hence, at more acidic pH values, the catalyst surface is positively charged, while above pH 6.3 it is negatively charged [32]. The second reason is due to the CIP zwitterion forming three different ionic forms, which mainly dependent on the pH value of the solution. The first dissociation constant (pK_1) of CIP was measured to be (6.15 ± 0.07) and the second (pK_2) was (8.66 ± 0.07) [33]. Thus, the higher the pH value, the more negative the molecule obtained in solution, facilitating the efficient adsorption of CIP onto TiO_2 [34] when the pH value is low than 6.3. Moreover, in weak alkaline, much hydroxyl radicals can also be generated by enough hydroxide ion [34]. The decrease of the rate constant at higher pH value 11.0 may be due to the repellent effect and the difficult adsorption of negative substrate onto negatively charged TiO_2.

3.3. Preliminary degradation mechanism of CIP

The degradation mechanism of CIP was elucidated from the HPLC and HPLC/MS/MS results coupled with theoretical calculations using the FEDs. The HPLC chromatogram of CIP degradation is shown in Fig. 6. Six degradation products were detected during photocatalytic degradation, and the relative peak areas of all intermediates exhibit similar change trends (Fig. 7). The peaks all increase dramatically during the first 20 min interval and then decrease rapidly with increased time. Although the exact concentrations of the intermediates were not determined accurately as we did not have authentic standards, these data are still

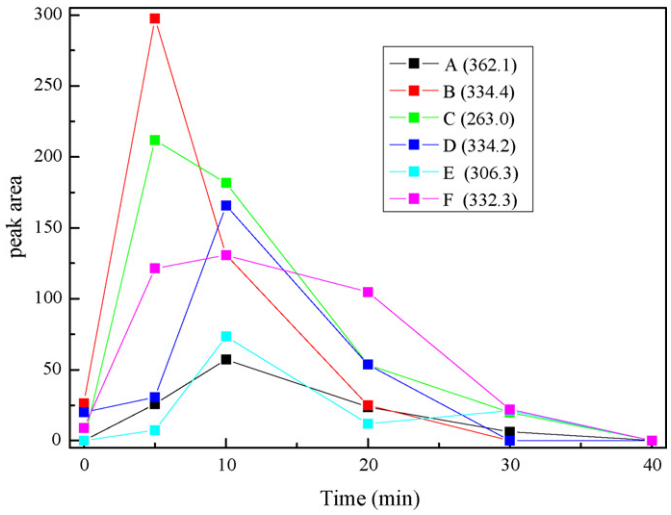

Fig. 7. Evolution and decay curves of degradation intermediates observed from HPLC analysis, with the conditions at 100 μM CIP, 1.5 g L^{-1} photocatalyst concentration.

very important for identification of the individual intermediates [35]. The corresponding molecular masses of all six intermediates were determined by using HPLC/MS/MS, and the retention time, mass spectra and structure of the identified intermediates are summarized in Table 2. The seventh intermediate, having a mass unit addition of 16 (M + 16, m/z 348, corresponding to the monohydroxyl derivatives) to the parent peak of CIP, was not found by HPLC/UV, but by ESI/MS-MS (also included in Table 2).

The frontier electron densities (FEDs) of CIP were also calculated to predict the reaction sites for electron extraction and hydroxyl radical attack, and the results are listed in Table 3. According to Frontier Orbital Theory, an electron can be easily extracted at positions with higher values of $2FED^2_{HOMO}$, while the addition of a hydroxyl radical is usually at a position with a higher $FED^2_{HOMO} + 2FED^2_{LUMO}$ value [36–38]. Thus, we first proposed that direct photo-hole (h^+) oxidation and hydroxylation were the two important pathways for CIP degradation. For direct photo-hole oxidation, the first reaction site was predicted based on the values of $2FED^2_{HOMO}$ [26,39]. C4 and N12 were found to be highest values, indicating that C4 or N12 should be the first site at which the electron is extracted. However, the C4 site appears to be unlikely due to stereo-hindrance effects. Thus, N12 is likely the main initial position for direct photo-hole oxidation of CIP. There were two intermediates with m/z values of 306 and 263 which had similar MS fragmentation patterns, and these are labeled C and E, respectively, in the HPLC chromatogram. Their MS fragments of (M+H)-18 and (M+H)-44 correspond to the loss of H_2O and CO_2, respectively, from the carboxylate group of the quinolone ring. These two intermediates are due to the partial and complete elimination, respectively, of the piperazynilic ring from the CIP molecule after hole attack on N12 [18,40], as shown in pathway 3 in Scheme 1. On the other hand, the first addition position of the •OH radical probably takes place on the atom with the highest $FED^2_{HOMO} + 2FED^2_{LUMO}$ value [26,39]. In this study, the values were found to be highest at the quinolone ring, and the most reasonable sites at which the addition of a hydroxyl radical could occur were C10 and C5. The intermediate product, G, resulted from hydroxyl radical attack at the C10 atom. Furthermore, two intermediates, A and B, that were more polar than CIP and another less polar

Table 2
Retention time, mass spectra and structure of the identified intermediates.

Intermediates	Retention time (min)	ES positive M+H	Chemical structure	m/z (relative intensity)
A	14.7	362	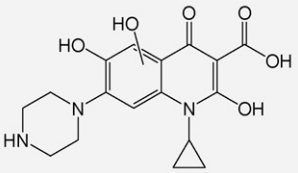	362 (100), 344 (60)
B	15.3	334	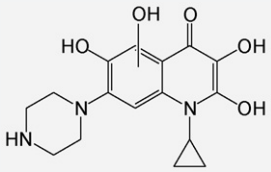	334 (100), 316 (50)
C	20.0	263	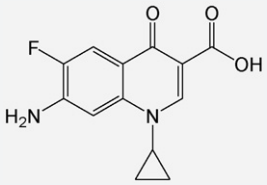	263 (40), 245 (100)
D	21.7	334	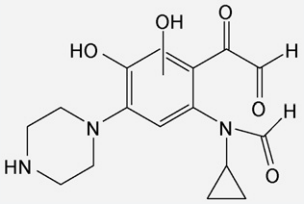	334 (28), 316 (100), 272 (30), 245 (8)

Table 2 (*Continued*)

Intermediates	Retention time (min)	ES positive M+H	Chemical structure	m/z (relative intensity)
E	23.4	306	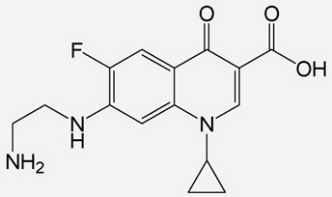	306 (27), 288 (100), 271 (10), 245 (98), 218 (22), 203 (30)
F	24.4	373	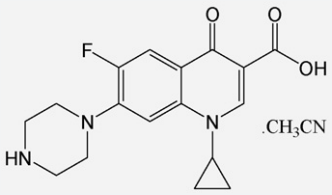	332 (95), 314 (20), 288 (100), 268 (15), 245 (50), 231 (15), 204 (8)
G	–	348	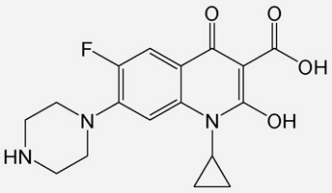	348 (100), 330 (10), 304 (32), 261 (19)

Table 3
Frontier electron densities on atoms of CIP calculated by using Gaussian 03 program at the B3LYP/6-31G* level.

Atom (number)	$2FED^2_{HOMO}$	$FED^2_{HOMO} + FED^2_{LUMO}$	Atom (number)	$2FED^2_{HOMO}$	$FED^2_{HOMO} + FED^2_{LUMO}$
C(1)	0.0818	0.1732	C(22)	0.0026	0.0069
C(2)	0.0152	0.1558	C(23)	0.0022	0.0074
C(3)	0.0958	0.0490	C(24)	0.0170	0.0134
C(4)	**0.2626**	0.1607	C(30)	0.0006	0.0050
C(5)	0.0192	**0.1986**	C(34)	0.0042	0.0910
C(6)	0.2148	0.1379	N(12)	**0.2260**	0.1333
C(9)	0.1088	0.0870	N(19)	0.0012	0.0022
C(10)	0.0012	**0.2561**	N(36)	0.1760	0.0107
C(13)	0.0088	0.0246	O(31)	0.0140	0.0025
C(14)	0.0026	0.0026	O(32)	0.0008	0.1807
C(15)	0.0036	0.0078	O(35)	0.1660	0.1549
C(17)	0.0078	0.0066	F(37)	0.0590	0.0323

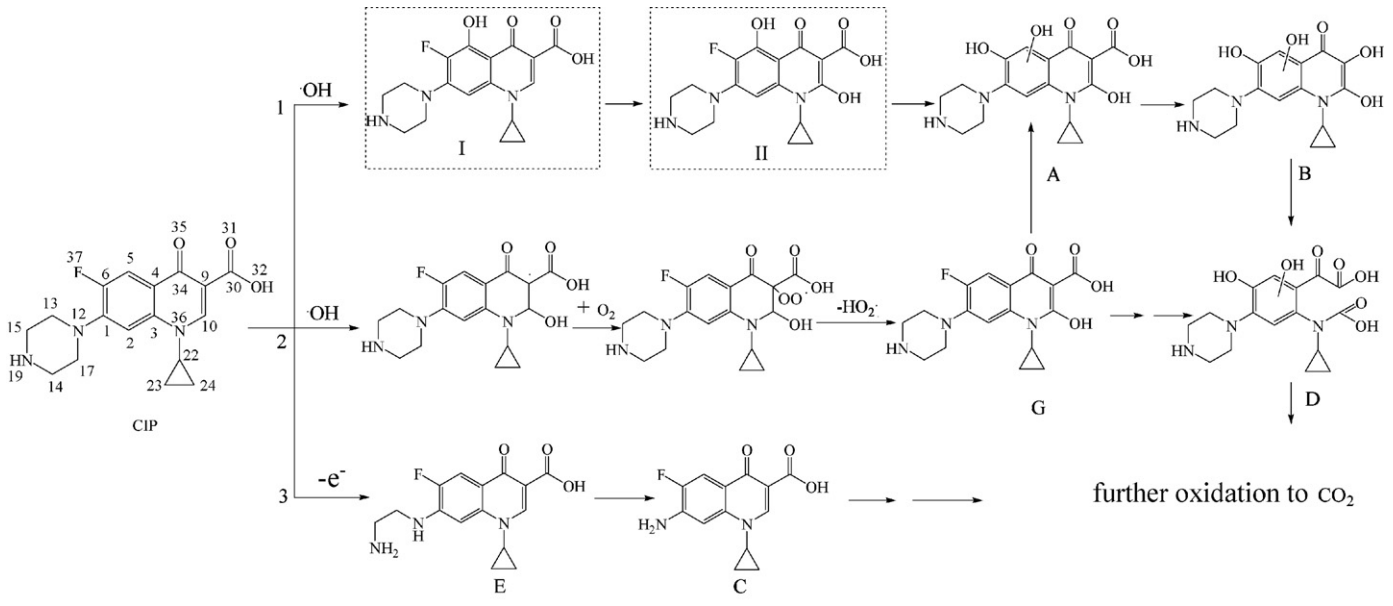

Scheme 1. Suggested mechanism for CIP degradation in TiO_2 photocatalysis.

intermediate, D, were also obtained in the next oxidation step and are shown in pathway 2 in Scheme 1. Intermediate A (m/z 362) resulted from oxidation of monohydroxyl intermediate G, with another hydroxyl radical addition to the parent molecule, while the F atom is also substituted with a hydroxyl radical. Two intermediates, B and D, with the same molecular weight (m/z 334) were also observed. Both of them have the MS fragments of (M+H)-18, but no group with (M+H)-44, suggesting the loss of a carboxylate group from the quinolone ring. After decarboxylation, A was oxidized to B. The intermediate D was produced by further oxidation of B, corresponding to the breakdown of its quinolone ring. However, intermediate I, resulting from $^{\bullet}$OH attack at C5, was not found. This phenomenon may be attributed to the rapid transformation of intermediate I to intermediate A through intermediate II, which is shown in pathway 1 in Scheme 1.

Although a lot of intermediates were detected during photocatalytic degradation, all the early intermediates and the hydroxylation intermediates would result in the breakdown of their quinolone ring structures with the further progress of degradation. As seen from Scheme 1, the addition of a hydroxyl radical to the parent molecule of CIP and the photo-hole direct attack are considered to be two reaction pathways for CIP degradation by photocatalysis.

4. Conclusions

The data presented provide fundamental information necessary for using AOPs to treat pharmaceuticals in aqueous waste streams. It appears that both oxidative and reductive processes could result in the effective removal of CIP from environmental waters because both $^{\bullet}$OH and $^{\bullet}N_3$ radicals, and hydrated electrons, can react with CIP with high rate constants of $(2.15 \pm 0.10) \times 10^{10}$, $(2.90 \pm 0.12) \times 10^{10}$ and $(2.65 \pm 0.15) \times 10^{10}$ M^{-1} s^{-1}, respectively. The short half-lives suggest that CIP can be degraded or decomposed quickly in the presence of a photocatalyst and illumination, and OH radical addition as well as the photo-hole attack is mainly responsible for the rapid oxidation of CIP in water. The results of this study indicate that AOPs, such as photocatalytic oxidation, is a cost-effective technology for removing pharmaceuticals from waters.

Acknowledgments

This is contribution No. IS-1143 from GIGCAS. The irradiation research was undertaken at the Radiation Laboratory, University of Notre Dame, U.S.A Department of Energy. The authors appreciate the selfless help and useful discussions from Prof. P.V. Kamat. Prof. Taicheng An also appreciate his award from Chinese Scholarship Council for his overseas visiting research and the financial supports from The Earmarked Fund of the State Key Laboratory of Organic Geochemistry (No. SKLOG2009A02), National Nature Science Foundation of China (No. 40973068), and Knowledge Innovation Program of Chinese Academy of Sciences (No. KZCX2-YW-QN103). This is contribution 45 from the Urban Water Research Center, University of California, Irvine.

References

[1] K. Kummerer, Pharmaceuticals in the Environment Sources, Fate, Effects and Risks, third ed., Springer, 2008.
[2] C.W. Knapp, L.A. Cardoza, J.N. Hawes, E.M.H. Wellington, C.K. Larive, D.W. Graham, Environ. Sci. Technol. 39 (2005) 9140–9146.
[3] O.A.H. Jones, N. Voulvoulis, J.N. Lester, Crit. Rev. Environ. Sci. Technol. 35 (2005) 401–427.
[4] H.C. Zhang, C.H. Huang, Environ. Sci. Technol. 39 (2005) 4474–4483.
[5] K. Ikehata, M. Gamal El-Din, S.A. Snyder, Ozone-Sci. Eng. 30 (2008) 21–26.
[6] A.J. Watkinson, E.J. Murby, S.D. Costanzo, Water Res. 41 (2007) 4164–4176.
[7] W.H. Xu, G. Zhang, X.D. Li, S.C. Zou, P. Li, Z.H. Hu, J. Li, Water Res. 41 (2007) 4526–4534.
[8] X.P. Nie, X. Wang, J. Chen, V. Zitko, T.C. An, Environ. Toxicol. Chem. 27 (2008) 168–173.
[9] K. Kummerer, A. Al-Ahmad, V. Mersch-Sundermann, Chemosphere 40 (2000) 701–710.
[10] I. Siminiceanu, M.M. Bobu, Rev. Chim-Bucharest 57 (2006) 1205–1209.
[11] R. Andreozzi, L. Campanella, B. Fraysse, J. Garric, A. Gonnella, R. Lo Giudice, R. Marotta, G. Pinto, A. Pollio, Water Sci. Technol. 50 (2004) 23–28.
[12] S.D. Cunningham, T.A. Anderson, A.P. Schwab, F.C. Hsu, Adv. Agron. 56 (1996) 55–114.
[13] K. Ikehata, N.J. Naghashkar, M.G. Ei-Din, Ozone-Sci. Eng. 28 (2006) 353–414.
[14] V.J. Pereira, K.G. Linden, H.S. Weinberg, Water Res. 41 (2007) 4413–4423.
[15] M.M. Haque, M. Muneer, J. Hazard. Mater. 145 (2007) 51–57.
[16] L.A. Cardoza, C.W. Knapp, C.K. Larive, J.B. Belden, M. Lydy, D.W. Graham, Water Air Soil Pollut. 161 (2005) 383–398.
[17] M.J. Lovdahl, S.R. Priebe, J. Pharmaceut. Biomed. 23 (2000) 521–534.
[18] K. Torniainen, J. Mattinen, C.P. Askolin, S. Tammilehto, J. Pharmaceut. Biomed. 15 (1997) 887–894.
[19] B. Dewitte, J. Dewulf, K. Demeestere, V.V. De Vyvere, P. De Wispelaere, H. Van Langenhove, Environ. Sci. Technol. 42 (2008) 4889–4895.
[20] G.V. Buxton, C.R. Stuart, J. Chem. Soc. Faraday Trans. 91 (1995) 279–281.
[21] A.R. Nicolaescu, O. Wiest, P.V. Kamat, J. Phys. Chem. A. 107 (2003) 427–433.
[22] W.H. Song, W.J. Cooper, S.P. Mezyk, J. Greaves, B.M. Peake, Environ. Sci. Technol. 42 (2008) 1256–1261.
[23] J. Peller, P.V. Kamat, J. Phys. Chem. A 109 (2005) 9528–9535.
[24] M. De Liguoro, C. Poltronieri, F. Capolongo, C. Montesissa, Chemosphere 68 (2007) 671–676.
[25] B.D. Lee, M. Iso, M. Hosomi, Chemosphere 42 (2001) 431–435.
[26] Y. Ohko, K.I. Iuchi, C. Niwa, T. Tatsuma, T. Nakashima, T. Iguchi, Y. Kubota, A. Fujishima, Environ. Sci. Technol. 36 (2002) 4175–4181.
[27] J. Peller, O. Wiest, P.V. Kamat, J. Phys. Chem. A 108 (2004) 10925–10933.
[28] M.S. Ram, D.M. Stanbury, Inorg. Chem. 24 (1985) 4233–4234.
[29] Z.B. Alfassi, W.A. Pruetz, R.H. Schuler, J. Phys. Chem. A 90 (1986) 1198–1203.
[30] R.E. Huie, C.L. Clifton, P. Neta, Radiat. Phys. Chem. 38 (1991) 477–481.
[31] G.V. Buxton, C.L. Greenstock, W.P. Helman, A.B. Ross, J. Phys. Chem. Ref. Data 17 (1988) 513–886.
[32] D.H. Kim, M.A. Anderson, J. Photochem. Photobiol. A: Chem. 94 (1996) 221–229.
[33] X.Q. Yu, G.L. Zipp, G.W.R. Davidson, Pharmaceut. Res. 11 (1994) 522–527.
[34] T.C. An, Y. Xiong, G.Y. Li, C.H. Zha, X.H. Zhu, J. Photochem. Photobiol. A: Chem. 152 (2002) 155–165.
[35] T. Paul, P.L. Miller, T.J. Strathmann, Environ. Sci. Technol. 41 (2007) 4720–4727.
[36] K. Fukui, T. Yonezawa, H. Shingu, J. Chem. Phys. 20 (1952) 722–725.
[37] H.H. Greenwood, J. Chem. Phys. 20 (1952) 1653–11653.
[38] K. Fukui, T. Yonezawa, C. Nagata, H. Shingu, J. Chem. Phys. 22 (1954) 1433–1442.
[39] X. Zhang, F. Wu, X.W. Wu, P.Y. Chen, N.S. Deng, J. Hazard. Mater. 157 (2008) 300–307.
[40] J. Burhenne, M. Ludwig, P. Nikoloudis, M. Spiteller, Environ. Sci. Pollut. Res. 4 (1997) 10–15.